ONE-IMAGE DEPTH-FROM-FOCUS FOR CONCENTRATION MEASUREMENTS

Peter Geißler
Interdisciplinary Center for Scientific Computing, University of Heidelberg
Im Neuenheimer Feld 368, D-69120 Heidelberg, Germany
Phone: (49) 06221-562826, email: pgeiss@davinci.iwr.uni-heidelberg.de

Bernd Jähne
Interdisciplinary Center for Scientific Computing, University of Heidelberg
Im Neuenheimer Feld 368, D-69120 Heidelberg, Germany
and
Scripps Institution of Oceanography, Physical Oceanography Research Division
University of California, La Jolla, CA 92093-0230, USA

KEY WORDS: Depth-from-Focus, 3D-Point Spread Function

ABSTRACT:

A one-image depth-from-focus technique for the measurement of the concentration and size distribution of small particles is described. The technique is based on a precise knowledge of the 3-D point spread function and requires objects of uniform brightness and simple shapes. The true area of the object and the distance from the focal plane is obtained from parameters such as the apparent (blurred) area of the object and the mean brightness in this area. The technique has been applied to measure the size distribution of bubbles submerged by breaking waves. A depth criterion is used to define a virtual measuring volume that is roughly proportional to the size of the bubbles.

1 INTRODUCTION

A novel depth-from-focus technique is introduced requiring only a single image. It has been developed to measure the concentration and size distribution of air bubbles submerged by breaking waves into the ocean with an optical sensor, but it is suitable also for other particles. The measurment of bubble concentrations and size distributions is an important oceanographic research topic, since they influence significantly various small scale air sea interaction processes and wave dynamics [4] [7].

To measure concentrations, the number and size of the bubbles and the measuring volume have to be known. The measuring volume can be determined from the 3D-positions of the observed bubbles. While it is trivial to get the position parallel to the image plane, the position along the optical axis can be determined by the simple fact that the blurring in the image increases with the distance from the focal plane. Most depth-from-focus techniques use several images of the scene - taken with different camera adjustments. Common methods are depth-series [2] or multi-aperture images [3] [9]. This types of multi-image approaches cannot be applied to scenes with moving objects without using several cameras simultaneously. In order to solve the depth-from-focus problem with just one image, it is important to note that the blurred image of an object is given by the convolution of it is well-focused image with the point spread function of the imaging optics. Therefore it is not possible to distinguish whether unsharpness in an image comes from blurring or from object properties such as smooth brightness changes. A priori knowledge of the point spread function and the properties of the observed objects is therefore necessary. Often a Gaussian shaped point spread function

10.5281/zenodo.14891

is assumed [8]. This approach cannot be followed in our application. In fact, the point spread function of our device does not even have rotational symmetry. On the other hand, like in many other applications, the type of objects that occur are precisely known. This paper describes a novel depth-from-focus technique based on the precise knowledge of the 3-D point spread function and the properties of the observed objects. No assumptions about the shape of the point spread functions are necessary.

2 OPTICAL SETUP

The air bubbles are visualized using a light blocking technique (Fig. 1). A CCD camera looks directly into the light source, which is a Halogen bulb or a pulsed LED array. A bubble entering the light beam refracts and reflects light in such a way that it is imaged as a black disk on a uniformly bright background. A short illumination time of 20 μs avoids motion blur. The images are stored on video tape or laser video disc for later processing. An area of typically $6 \times 8\,\mathrm{mm}^2$ is imaged on 240×512 pixel images with a spatial resolution of $27\,\mu\mathrm{m} \times 15\,\mu\mathrm{m}$. The measuring volume is at most several cm deep. The visualization system has been described in more detail by [5].

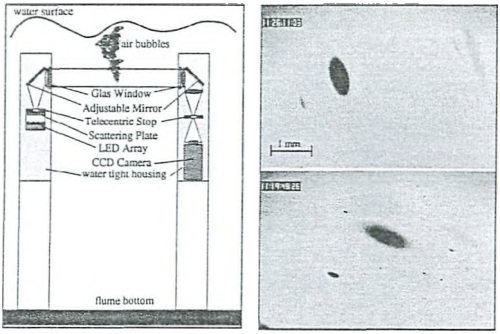

Figure 1: *left: Sketch of the optical bubble measuring device used at linear flume in Delft. The light source and the optical receiver with CCD camera are mounted 5–20 cm below the water surface. The free optical path between source and receiver is about 50 cm. The measuring volume is located in the middle of this path. right: Air bubbles at several cm beneath the mean water surface.*

3 MODEL OF IMAGE FORMATION

An air bubble can be modelled by its light absorbing coefficient $\tau(\vec{x})$ in the object plane. A circular bubble at the position $\vec{X}_0$ and with the radius r is then described as a circular box function $\tau(\vec{X}) = \Pi\left(|\vec{X} - \vec{X}_0|/2r\right)$ where $\Pi(x)$ is the unit step function. The capital letters indicate object plane coordinates. The Z axis of the system coincides with the optical axis of the system. The image of the bubble is given by the convolution of the well focused image with the *point spread function* $PSF(\vec{x})$ of the optical system:

$$I(\vec{x}) = \left(1 - \Pi\left(\frac{|\vec{x} - \vec{x}_0|}{2r'}\right)\right) * PSF(\vec{x}). \tag{1}$$

In this equation, the object coordinates have been replaced by the image coordinates. The radius of the bubble at the image plane is given by $r' = V_g(z)r$, where V_g is the geometrical magnification factor. It is not possible to use a simple model (like a box or Gaussian function) for the point spread function of our optical system. Since the filament of the halogen bulb is imaged on the receiver lens diaphragm, its image forms the effective diaphragm of the system. Therefore, the shape of the point spread function is given by the irradiance at the lens diaphragm which is, except for a size factor, equal to the brightness distribution

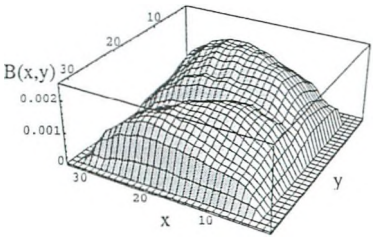

Figure 2: *Pseudo-3D plot of the irradiance distribution $B(x, y)$ at the diaphragm of the receiver lens. The resulting point spread function shows two maxima. The larger one comes from the direct imaging of the filament, the smaller one from the image reflected by a spherical mirror.*

$B(\vec{x})$ on the filament of the halogen bulb. Thus, the normalized PSF can be written as

$$PSF_z(\vec{x}) = kB\left(\frac{1}{V_p(z)}\vec{x}\right) \tag{2}$$

with the normalization factor $k^{-1} = \int d\vec{x}B(\vec{x})$. At the focal plane ($z = 0$) V_p is zero, resulting in a delta function for the PSF. The resulting brightness distribution on the CCD sensor plane is then

$$I(\vec{x}) = v(\vec{x})\left[1 - \tau\left(\frac{1}{V_g(z)}\vec{x}\right) * PSF_z(\vec{x})\right] \tag{3}$$

with $v(\vec{x})$ being the vignetting function.

4 DETERMINATION OF THE CONCENTRATION BY DEPTH-FROM-FOCUS

4.1 Low Level Preprocessing

For the depth-from-focus technique it is critical that the gray values in the images are known absolutely and are independent of the actual brightness of the illumination and the actual settings of the camera and frame grabber.
A linear illumination model is applied assuming that the image shows a background level $b(\vec{x})$ and that the measured gray values $g(\vec{x})$ are further proportional to the irradiance $I(\vec{x})$. Then

$$g(\vec{x}) = a(\vec{x})I(\vec{x}) + b(\vec{x}). \tag{4}$$

The unknown quantities $b(\vec{x})$ and $a(\vec{x})$ are obtained by taking a background image $g_b(\vec{x})$ with illumination switched off ($I(\vec{x}) = 0$) and a zero image $g_z(\vec{x})$ in which no bubbles are present ($I(\vec{x}) = I_0(\vec{x})$). Then the linear inhomogeneous point operation

$$n(\vec{x}) = \frac{g_z(\vec{x}) - g(\vec{x})}{g_z(\vec{x}) - g_b(\vec{x})} \tag{5}$$

results in a normalized gray value $n(\vec{x})$ in the range of 0 to 1. It is important to note that this procedure removes any type of inhomogeneities caused by uneven illumination or small dust particles on the CCD chip or the lenses. Applying Eq. 5 to Eq. 3, one yields

$$n(\vec{x}) = \tau\left(\frac{1}{V_g(z)}\vec{x}\right) * PSF_z(\vec{x}). \tag{6}$$

for the normalized image.

4.2 Determination of Size and Distance from Focal Plane

With increasing blurring, the edges of the bubble become less steep, the radius (defined at the gray values that are $1/e$ of the maximum gray value) increases, and finally also the maximum gray value decreases. Figure 3 illustrates these effects by showing the $1/e$ area and its mean gray value as a function of the distance z from the focal plane. In order to describe the blurring, two parameters of the bubbles are measured:

$1/e$ radius r_e : For small blurring, this is a good approximation for the true radius of the bubble. It increases with increasing blurring. In case of elliptically shaped bubbles, an equivalent radius was computed from the area.

Mean gray value of the $1/e$ area (g_e) : This parameter is a good integral measure of the blurring. It decreases with increasing blurring.

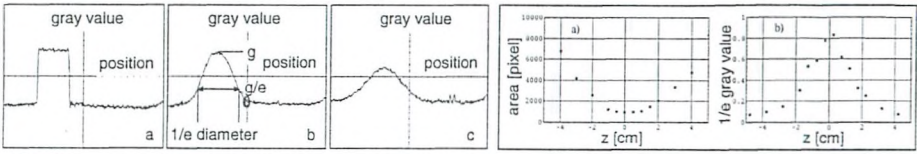

Figure 3: *left: Radial cross section through the gray value distribution of bubbles at different distances from the focal plane. The distance increases from a) to c). right: $1/e$ area (a) and its mean gray value (b) as a function of the distance z from the focal plane for a bubble with 0.25 mm radius.*

The basic idea of our approach is to use these two parameters r_e and g_e to infer the two quantities of interest: the true radius, r, and and distance from the focal plane, z. For a given point spread function, there is a unique and monotonic relation for r and z as a function of r_e and g_e. These relations can be computed from the known point spread function and the magnification factors $V_g(z)$ and $V_p(z)$. Both were calculated from the setup of the optical system using geometric optics. Using Eq. 6, the normalized images $n(\vec{x})$ of bubbles of different sizes and distances from the focal plane were computed. These images were segmented to obtain both r_e and g_e. In a second step, the values for $r(r_e, g_e)$ and $z(r_e, g_e)$ were mapped on a regular grid in (r_e, g_e) coordinates and stored in look-up tables (Fig. 4 left). There is an intrinsic ambivalence in this measurement: it is impossible to distinguish if a bubble is located in front or behind the focal plane. This results in an ambivalence in the bubble size measurement, for the distance information is needed to reconstruct the true size of blurred bubbles. The effects are small and not significant if only size distributions are computed. Since the probability for a bubble to occur in front and behind the focal plane is the same, we can simply take the mean value of the relations for positive and negative z. To overcome this problem, we now use a second generation device with a telecentric path of rays. The LUTs for positive and negative distances from the focal plane become then identical if further the $1/2$ area is used as blurred size instead of the $1/e$ area.

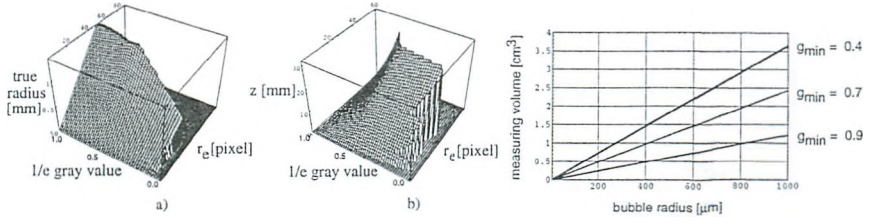

Figure 4: *left: True bubble radius, r, (a) and distance from the focal plane, z, (b) as a function of the mean $1/e$ gray value g_e and the $1/e$ radius r_e. right: Measuring volume as a function of bubble radius for three different values of the lower gray value limit g_{min}*

4.3 Determination of the Radius-dependent Measuring Volume

Because of the decreasing of the mean gray value with increasing distance from the focal plane, the measuring volume can now be defined by a lower limit for g_e. Only bubbles with gray values above this limit are processed. All bubbles with the same ratio between the geometrically magnified radius and the size of the point spread function have the same mean gray value g_e, because of the similarity of their images. Thus

$$\frac{rV_g(z)}{V_p(z)} = const \Leftrightarrow g_e = const. \tag{7}$$

Denoting the constant in the above equation by $\gamma(g_e)$, the volume boundaries z_b for the lower limit g_e^* become

$$z_b = \gamma(g_e^*)\,\nu^{-1}(r) \quad with \quad \nu(r) = \frac{V_p(z)}{V_g(z)}. \tag{8}$$

In general, the solutions for positive and negative values of z are different. However, with the optical setup used in our device, $\nu(z) \sim |z|$ and therefore $|z_b| = \gamma(g_e^*)r$, yielding symmetric volume boundaries (Fig. 4 right).

4.4 Implementation of Image Processing Algorithms

An effective implementation of the depth-from-focus technique to measure the size distribution consists of the following five steps:

- The measured point spread function and the calculated magnification factors $V_g(z)$ and $V_p(z)$ are used to compute the true bubble radius and the distance from the focal plane as a function of the $1/e$ radius and the mean gray value. These computations are quite time consuming but only have to be done once for a given optical setup. The results are stored in 2-D look-up tables for further quick reference (Fig. 4a).
- Gray-scale normalization and segmentation.
- Computation of the $1/e$ radius and the mean gray value.
- Computation of the true radius and distance from the focal plane using the previously computed 2-D lookup tables.
- Computation of the size distribution of the bubbles.

Using a i860 RISC processor board with real-time image transfer to a frame grabber, it took only 1–2 s per image to perform all the steps except for the first one. The segmentation algorithm used consists of two main steps. In order to localize the object, the image is binarized with a global threshold. For each object, the pixel with maximum gray value is chosen as starting point for the following region growing. Using a modified version of the region growing algorithm developed by [6], the $1/e$ area of each object is then segmented. Therefore, the value of the threshold does not influence the result of the segmentation. It only must be higher than the minimum value for g_e.

5 RESULTS

As an example, the results of the analysis of two series of 600 and 400 images respectively, are shown in Fig. 5. The images were taken in the large wind/wave flume at Delft Hydraulics (The Netherlands) to explore the potential of the new technique. Image sequences were recorded on a S-VHS video recorder and later processed at the Institute for Environmental Physics in Heidelberg. The instrument was mounted 5 cm below the mean water surface. Measurements were conducted at wind speeds of 11 m/s and 14 m/s. The results nicely show the steep decrease in the bubble density towards larger radii and are in good agreement with measurements taken by [1].

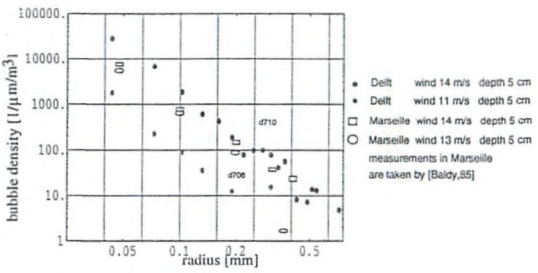

Figure 5: *Size distribution of bubbles measured at a wind speed of 14 m s and 5 cm below the mean water surface in the wind/wave flume of Delft Hydraulics, The Netherlands.*

6 CONCLUSIONS

In this paper it has been showed that depth-from-focus techniques can be used with only one image provided that a precise knowledge of the shape of the object is known and that an adequate illumination and low-level image processing has been performed. The size and the distance of bubbles from the focal plane could be measured from only one image. Bubbles are quite simple objects in the sense that they have an elliptic shape. Although we have demonstrated the technique only with these simple objects, we feel that it opens the way to further research in one-image depth-from-focus. Counting cells in bioreactors is already another successful application of a different one-image depth-from-focus technique developed in our research group by [10]. The next logical step of research would be to extend these techniques to more complex and general object shapes.

ACKNOWLEDGEMENTS

Financial support by the National Science Foundation (OCE89 11224), the Office of Naval Research (N00014-89-J-3222), and the European Community (Large Installation Program) is gratefully acknowledged.

REFERENCES

[1] Baldy, S., Bouruel M.: 1985, 'Measurements of Bubbles in a Stationary Field of Breaking Waves by a Laser Based Single-Particle Scattering Technique' *Journal of Geophysical Research, Vol. 90 No. 1*

[2] Darell, T., Wohn, K.: 1990, 'Depth-from-focus using a pyramid architecture', *Pattern Recognition Letters, 11, 787–796*

[3] Ens, J., Lawrence, P.: 1993, 'An investigation of methods for determining depth-from-focus' , *IEEE Trans. PAMI, 15, 97–108*

[4] Farmer, D. M., McNeil, C. L., Johnson, B. D.: 1993, 'Evidence for the importance of bubbles in increasing air-sea gas flux' , *Nature, 361, 620–623*

[5] Geißler, P., Jähne, B.: 1994, 'An Imaging Optical Technique for Bubble Measurements', *3rd international meeting on natural physical processes related to sea surface sound, Lake Arrowhead, CA*

[6] Hering, F., Merle, M., Wierzimok,D., Jähne, B.: 1995, 'A Robust Technique for Tracking Particles over Long Image Sequences', *to be published in Proc. of ISPRS Intercommission Workshop 'From Pixels to Sequences', Zurich, March 22 - 24. In Int'l Arch. of Photog. and Rem. Sens., Vol 30, Part 5W1*

[7] Lamarre, E., Melville, W. K.: 1991, 'Air Entrainment and dissipation in breaking waves', *Nature, 351, 469–472*

[8] Lai, S. H., Fu , C. W., Chang, S. Y.: 1992, 'A generalized Depth Estimation Algorithm', *IEEE Trans. PAMI, 14, 405–411*

[9] Pentland, A. P.: 1987, 'A new sense for depth of field', *IEEE Trans. PAMI, 9, 523–531*

[10] Scholz, T., Jähne, B., Suhr, H., Wehnert, G., Geißler, P., Schneider, K.: 1994, 'A New Depth-from-Focus Technique for In Situ Determination of Cell Concentration in Bioreactors', *Proceedings of the 16th DAGM Symposium, Wien, 145–154*